NASA-CR-195140

Report No: TRC-EM-CAB-9402

IN 32 CR
205063
30 P

HIGH-FREQUENCY TECHNIQUES FOR RCS PREDICTION OF PLATE GEOMETRIES AND A PHYSICAL OPTICS/EQUIVALENT CURRENTS MODEL FOR THE RCS OF TRIHEDRAL CORNER REFLECTORS

Semiannual Progress Report

PART I

Constantine A. Balanis and Lesley A. Polka

August 1, 1993 - January 31, 1994

PART II

Constantine A. Balanis and Anastasis C. Polycarpou

August 1, 1993 - January 31, 1994

Telecommunications Research Center
College of Engineering and Applied Science
Arizona State University
Tempe, AZ 85287-7206

Grant No. NAG-1-562
National Aeronautics and Space Administration
Langley Research Center
Hampton, VA 23665

N94-24616
Unclas
0205063
(NASA-CR-195140) HIGH-FREQUENCY TECHNIQUES FOR RCS PREDICTION OF PLATE GEOMETRIES AND A PHYSICAL OPTICS/EQUIVALENT CURRENTS MODEL FOR THE RCS OF TRIHEDRAL CORNER REFLECTORS, PARTS 1 AND 2 Semiannual Progress Report, 1 Aug. 1993 - 31 Jan. 1994 (Arizona State Univ.) 30 p
H1/32

Report No: TRC-EM-CAB-9402

HIGH-FREQUENCY TECHNIQUES FOR RCS PREDICTION OF PLATE GEOMETRIES AND A PHYSICAL OPTICS/EQUIVALENT CURRENTS MODEL FOR THE RCS OF TRIHEDRAL CORNER REFLECTORS

Semiannual Progress Report

PART I

Constantine A. Balanis and Lesley A. Polka

August 1, 1993 - January 31, 1994

PART II

Constantine A. Balanis and Anastasis C. Polycarpou

August 1, 1993 - January 31, 1994

Telecommunications Research Center
College of Engineering and Applied Science
Arizona State University
Tempe, AZ 85287-7206

Grant No. NAG-1-562
National Aeronautics and Space Administration
Langley Research Center
Hampton, VA 23665

Abstract

Part I of this report includes formulations for scattering from the coated plate and the coated dihedral corner reflector. A coated plate model based upon the Uniform Theory of Diffraction (UTD) for impedance wedges was presented in the last report. In order to resolve inaccuracies and discontinuities in the predicted patterns using the UTD-based model, an improved model that uses more accurate diffraction coefficients is presented in this report. A Physical Optics (PO) model for the coated dihedral corner reflector is presented as an intermediary step in developing a high-frequency model for this structure. The PO model is based upon the reflection coefficients for a metal-backed lossy material. Preliminary PO results for the dihedral corner reflector suggest that, in addition to being much faster computationally, this model may be more accurate than existing moment method (MM) models.

Part II of this report presents an improved Physical Optics (PO) / Equivalent Currents model for modeling the Radar Cross Section (RCS) of both square and triangular, perfectly conducting, trihedral corner reflectors. The new model uses the PO approximation at each reflection for the first- and second-order reflection terms. For the third-order reflection terms, a Geometrical Optics (GO) approximation is used for the first reflection; and PO approximations are used for the remaining reflections. The previously reported model used GO for all reflections except the terminating reflection. Using PO for most of the reflections results in a computationally slower model because many integrations must be performed numerically, but the advantage is that the predicted RCS using the new model is much more accurate. Comparisons between the two PO models, Finite-Difference Time-Domain (FDTD) and experimental data are presented for validation of the new model.

I. HIGH-FREQUENCY TECHNIQUES FOR RCS PREDICTION OF PLATE GEOMETRIES

A. INTRODUCTION

Recent reports [1, 2, 3, 4, 5, 6, 7, 8] have dealt with the use of the Uniform Theory of Diffraction (UTD) for impedance wedges [9, 10] to model the principal-plane radar cross section (RCS) of a coated conducting plate. The initial goal was to apply the knowledge gained from modeling this simple structure to more complicated geometries, specifically the coated dihedral corner reflector. As the modeling process has evolved, however, the importance of modeling the plate has grown as a problem in and of itself, independent from the dihedral corner reflector problem. Specifically, the UTD plate model presented in the previous report [1] yielded fairly good results near and at normal incidence; however, angles closer to the transition regions, near grazing incidence, presented problems. The problems involved inaccuracies and discontinuities in the predicted patterns in the regions near the transition from the coated side to the uncoated side of the plate. The resolution of these problems requires the use of more accurate diffraction coefficients in these regions. Modifications to the model presented in the last report are discussed in this report.

Because diffraction terms are the predominant contributors to the overall RCS of the coated plate, the formulation of an accurate high-frequency model for this geometry requires careful analysis of diffraction mechanisms and methods of modeling various diffraction mechanisms for coated structures. The information garnered from this analysis is useful for applications to other coated structures for which diffractions are the predominate contribution to the overall RCS; however, this analysis is not very useful for the analysis of the coated dihedral corner reflector because the main scattering mechanisms for this structure are single and double

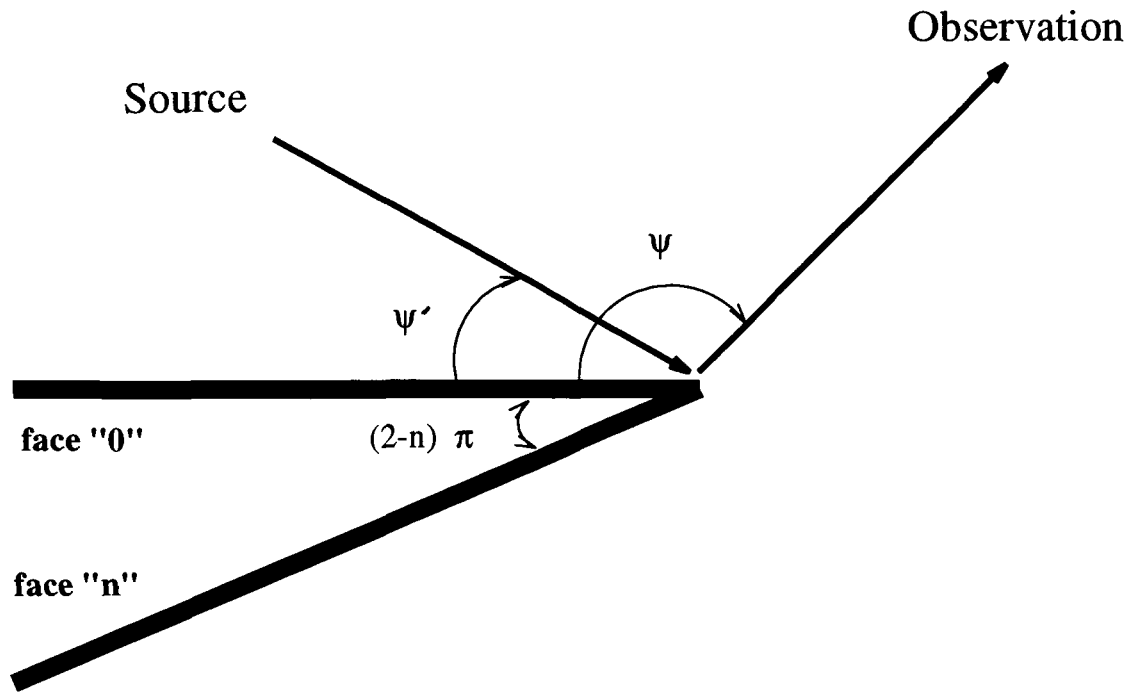

Figure 1: Impedance wedge geometry.

reflections. In order to resolve inaccuracies in a previously reported UTD model for the coated dihedral corner reflector [11], a Physical Optics (PO) model for this structure is presented in this report. Results are compared to Moment Method (MM) data.

B. THEORY AND RESULTS

1. Coated Plate - UTD Analysis

The UTD model for coated plate scattering presented in the previous report [1] used the UTD diffraction coefficients formulated by Tiberio, *et al.* , and Griesser and Balanis [9, 10] for an impedance wedge, shown in Fig. 1. The coated plate, shown in Fig. 2, was modeled as the joining of two half planes with a coating of finite thickness on the upper wedge faces. The coating was incorporated into the model using an equivalent impedance approximated by the impedance of a comparable short-circuited transmission-line. Results presented in the last report demonstrated that the UTD model formulated in this manner is very accurate for

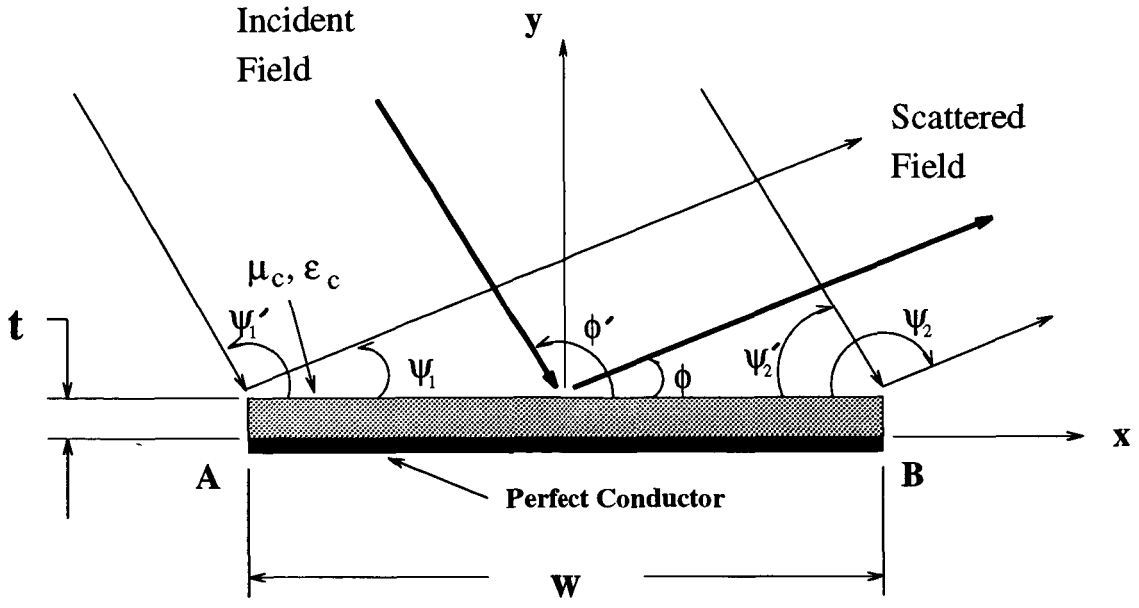

Figure 2: Geometry for principal-plane scattering from a strip/plate with a finite-thickness coating backed by a perfect conductor.

most scattering angles. The necessity of incorporating higher-order diffraction and surface-wave terms was also demonstrated.

Terms accounting for multiple diffractions between the edges improve the model; however, the way in which these terms were incorporated into the model presented in the last report leads to inaccuracies and discontinuities in the region of transition from the coated to the uncoated side of the plate. Specifically, the diffraction coefficient for the impedance wedge goes to zero when the source is on the face of the wedge and for the reciprocal case of an observation point on the wedge face. In order to use this coefficient for higher-order diffractions, the coefficient was calculated for a point slightly off the wedge face. This worked remarkably well for most scattering angles; however, improvement in the grazing regions is desired.

To more effectively account for higher-order diffractions, a more precise coefficient that does not go to zero on the face of the wedge must be used. Tiberio, *et al.*, formulated the necessary diffraction coefficient in [9]. The general form of the resulting diffracted field is given in Eq. (16) of [9]. This can be greatly simplified

for the case of a half plane [12] so that the resulting expression that will be included in a new version of the UTD model for the coated plate is:

$$
\begin{aligned}
\mathbf{E_d} &= \mathbf{E_i}\frac{e^{-j(k\rho+\frac{\pi}{4})}}{\sqrt{2nk\rho}}\left(\frac{\sin\phi}{1+\cos\theta_2}\right)\frac{\sin\left(\frac{\theta_0-3\pi}{4}\right)\sin\left(\frac{\theta_2-\pi}{4}\right)}{\sin\left(\frac{\theta_0-\phi'}{4}\right)\sin\left(\frac{\theta_2+\phi'-2\pi}{4}\right)} \\
&\times \frac{\psi_2\left(\frac{5\pi}{2}-\phi+\theta_0\right)\psi_2\left(\frac{-\pi}{2}-\theta_0\right)\psi_2\left(\frac{\pi}{2}+\phi+\theta_2\right)\psi_2\left(\frac{3\pi}{2}-\theta_2\right)}{\psi_2\left(\frac{5\pi}{2}-\phi-\theta_0\right)\psi_2\left(\frac{-\pi}{2}+\theta_0\right)\psi_2\left(\frac{\pi}{2}+\phi-\theta_2\right)\psi_2\left(\frac{3\pi}{2}+\theta_2\right)} \\
&\times \frac{F[2k\rho\cos^2(\phi/2)]-F[2k\rho\sin^2(\theta_2/2)]}{\cos^2(\phi/2)-\sin^2(\theta_2/2)} \\
&\times \left(1+\sin\theta_2\left[f_2(\frac{3\pi}{2}-\theta_0)+f_2(\frac{\pi}{2}+\theta_0)\right.\right. \\
&+ \left.\left. f_2(\frac{-\pi}{2}-\theta_2)+f_2(\frac{-3\pi}{2}+\theta_2)+\frac{1}{2\cos(\phi/2)}\right]\right) \qquad (1)
\end{aligned}
$$

The usual definitions for the variables apply; *i.e.*, $\theta_{0,2}$ are the Brewster angles for the designated faces, ϕ' is the angle of incidence, ϕ is the angle of observation, ρ is the distance between diffraction points, $F[x]$ is the Fresnel transition function extended to complex arguments as explained in [12], and $f_2(t)$ is the expression:

$$f_2(t) = -\frac{\pi\sin t - 2\sqrt{2\pi}\sin(t/2)+2t}{8\pi\cos t} \qquad (2)$$

In general, $f_n(t)$ is an infinite integral [9]. Fortunately, this integral reduces to closed form for the case of a half plane ($n=2$) and is given above as $f_2(t)$.

This updated version of the UTD model will be coded in the next reporting period and numerical results obtained and compared to measured data. Another modification that will be explored is the use of the diffraction coefficients reported in [13, 14]. These coefficients are for cylindrical-wave incidence and should model interactions between edges more accurately than the previously used coefficients, which are theoretically only for plane-wave incidence on a wedge.

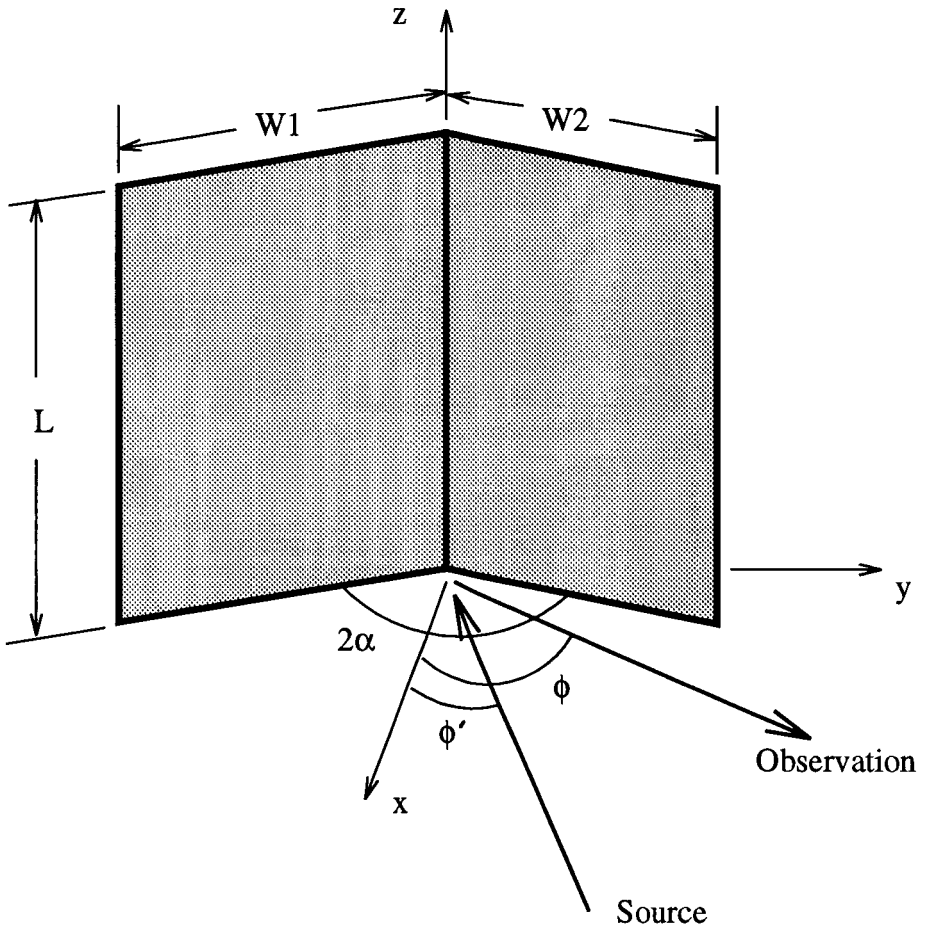

Figure 3: Dihedral corner reflector geometry.

2. Coated Dihedral Corner Reflector

The coated dihedral corner reflector, shown in Fig. 3, is an important structure to analyze because it supports most of the basic scattering mechanisms. Specifically, mechanisms which must be included in a high-frequency RCS model are first-order diffractions for both exterior and interior wedges; single, double, and triple reflections; and reflection-diffraction terms. The most logical approach to formulating a high-frequency model for this geometry is to combine UTD, to account for diffractions, and Geometrical Optics (GO), to account for reflections. This model was formulated and reported on by Griesser, *et al.*, in [11]; however, since the appearance of this paper, inaccuracies due to the reflection terms have been discovered [7]. In order to isolate the source of the inaccuracy, a PO model for the reflector

is examined in this report. Although the PO model cannot account for diffraction mechanisms, it is a good model to use to study the reflector because reflection terms dominate the scattering pattern of this geometry. A brief summary of the model is given in the next section, followed by a results section, which includes MM data for comparison. In addition to being a computationally intensive model, the MM model is also highly inaccurate at some points. These difficulties with the MM model further emphasize the need for an accurate high-frequency model for the coated dihedral corner reflector.

PO Analysis: The PO model for the coated reflector is based upon the PO model for the perfectly conducting reflector, reported upon in [15]. Obtaining results for the coated reflector simply involves multiplying the fields for the perfectly conducting geometry by the appropriate reflection coefficients. The reflection coefficient for a coated, flat plane backed by a perfect conductor is used as the fundamental reflection coefficient. The short-circuited transmission-line approximation is used to account for the coating impedance. The expressions for the basic reflection coefficients are, thus, given by:

Soft Polarization

$$\Gamma(\theta) = \frac{\eta_{eq}\cos\theta - \sqrt{\frac{1-\sin^2\theta}{\mu_c\epsilon_c}}}{\eta_{eq}\cos\theta + \sqrt{\frac{1-\sin^2\theta}{\mu_c\epsilon_c}}} \tag{3}$$

Hard Polarization

$$\Gamma(\theta) = \frac{-\cos\theta + \eta_{eq}\sqrt{\frac{1-\sin^2\theta}{\mu_c\epsilon_c}}}{\cos\theta + \eta_{eq}\sqrt{\frac{1-\sin^2\theta}{\mu_c\epsilon_c}}} \tag{4}$$

where

$$\eta_{eq} = j\sqrt{\frac{\mu_c}{\epsilon_c}}\tan\left(2\pi t\sqrt{1-\sin^2\theta}\right) \tag{5}$$

The angle of incidence with respect to the surface normal is θ; μ_c and ϵ_c are the relative permeability and permittivity, respectively, of the coating material; and t is the coating thickness in free-space wavelengths.

Coefficients for multiple reflections are formed as a product of this basic coefficient. To obtain the appropriate reflection terms for each plate of the reflector, the incident angles measured from the normal to each plate must be known at each reflection. The reflection coefficients are a product of the basic coefficient from above evaluated at the appropriate angles. The following table summarizes the reflection coefficients for single, double, and triple reflections from both plates of the reflector. Referring to Fig. 3, the left-hand plate is Plate I and the right-hand plate is Plate II. The angle of incidence with respect to the given coordinate system is ϕ; and α is half of the total interior angle between the plates of the reflector.

Table of Reflection Coefficients

Angular Range	Angle to the Normal	Reflection Coefficent
Plate I - Single Reflection		
$-\frac{\pi}{2} \leq \phi < -\alpha$	$\theta_I = \frac{\pi}{2} + (\phi + \alpha)$	$\Gamma(\theta_I)$
$-\alpha \leq \phi < 0$	$\theta_I = \frac{\pi}{2} - (\phi + \alpha)$	$\Gamma(\theta_I)$
$0 \leq \phi < (\frac{\pi}{2} - \alpha)$	$\theta_I = \frac{\pi}{2} - (\phi + \alpha)$	$\Gamma(\theta_I)$
$(\frac{\pi}{2} - \alpha) \leq \phi \leq \frac{\pi}{2}$	$\theta_I = -\frac{\pi}{2} + (\phi + \alpha)$	$\Gamma(\theta_I)$
Plate II - Single Reflection		
$-\frac{\pi}{2} \leq \phi < (\alpha - \frac{\pi}{2})$	$\theta_{II} = -\frac{\pi}{2} - (\phi - \alpha)$	$\Gamma(\theta_{II})$
$(\alpha - \frac{\pi}{2}) \leq \phi < 0$	$\theta_{II} = \frac{\pi}{2} + (\phi - \alpha)$	$\Gamma(\theta_{II})$
$0 \leq \phi < \alpha$	$\theta_{II} = \frac{\pi}{2} + (\phi - \alpha)$	$\Gamma(\theta_{II})$
$\alpha \leq \phi \leq \frac{\pi}{2}$	$\theta_{II} = \frac{\pi}{2} - (\phi - \alpha)$	$\Gamma(\theta_{II})$
Plate I - Double Reflection		
$-\frac{\pi}{2} \leq \phi \leq \frac{\pi}{2}$	$\theta_{I_{2nd}} = 2\alpha - \theta_{II}$	$\Gamma(\theta_{II})\Gamma(\theta_{I_{2nd}})$
Plate II - Double Reflection		
$-\frac{\pi}{2} \leq \phi \leq \frac{\pi}{2}$	$\theta_{II_{2nd}} = 2\alpha - \theta_I$	$\Gamma(\theta_I)\Gamma(\theta_{II_{2nd}})$
Plate I - Triple Reflection		
$-\frac{\pi}{2} \leq \phi \leq \frac{\pi}{2}$	$\theta_{I_{3rd}} = 4\alpha - \theta_I$	$\Gamma(\theta_I)\Gamma(-\theta_{II_{2nd}})\Gamma(\theta_{I_{3rd}})$
Plate II - Triple Reflection		
$-\frac{\pi}{2} \leq \phi \leq \frac{\pi}{2}$	$\theta_{II_{3rd}} = 4\alpha - \theta_{II}$	$\Gamma(\theta_{II})\Gamma(-\theta_{I_{2nd}})\Gamma(\theta_{II_{3rd}})$

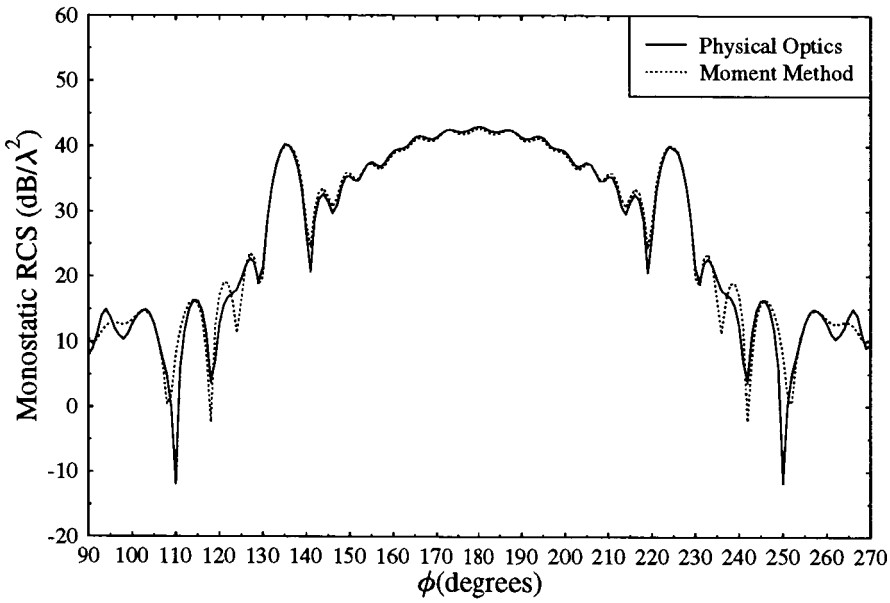

Figure 4: Monostatic RCS of a perfectly conducting dihedral corner reflector ($W1 = W2 = L = 5.6088\lambda$, $2\alpha = 90°$, soft polarization).

Results: Experiments are currently in progress to obtain measured RCS data for various dihedral corner reflector geometries. Both conductors and coated conductors are being used, and both polarizations are being considered. The coatings that are being studied are electrically thin and lossy. These results will be presented in the next reporting period.

Preliminary results that illustrate the validity of using the PO model presented in the last section are shown in Figs. 4 and 5. The geometry is rotated 180° from that of Fig. 3 so that the reflector is situated in the region $135° \leq \phi \leq 215°$. In other words, $\phi = 180°$ in Figs. 4 and 5 corresponds to $\phi = 0°$ in Fig. 3, where the corner would analogously be situated in the region $-45° \leq \phi \leq 45°$. In Fig. 4 PO and MM results are compared for a perfectly conducting reflector. The high accuracy of the PO results demonstrates that reflections are the predominate scattering mechanisms for this geometry; and because of this, the PO model should

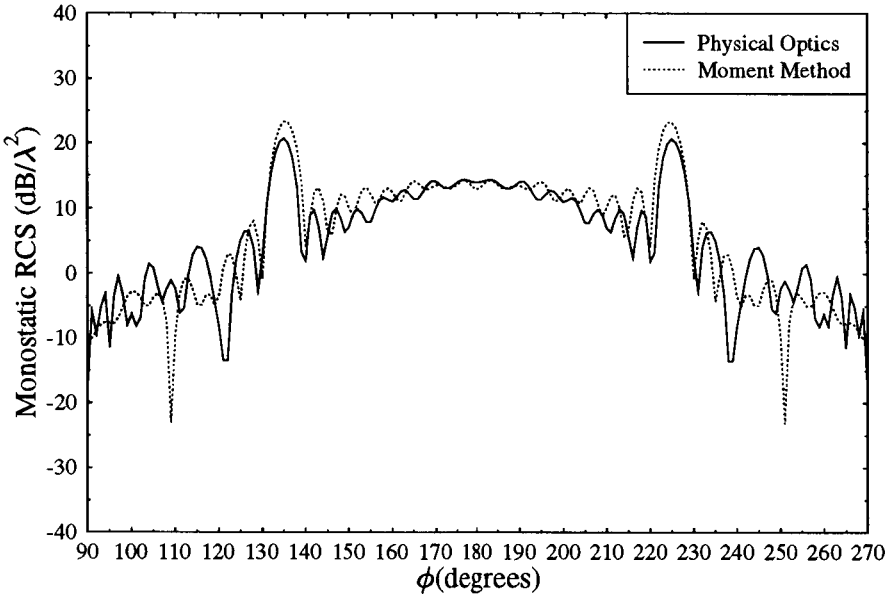

Figure 5: Monostatic RCS of a coated conducting dihedral corner reflector ($W1 = W2 = L = 5.6088\lambda$, $2\alpha = 90°$, soft polarization, coating: $t = 0.065\lambda$, $\mu_c = 1.5 - j0.7$, $\epsilon_c = 7.8 - j1.6$).

yield fairly accurate results for the coated reflector also.

Fig. 5 contains PO and MM results for a coated reflector. A rough analysis reveals that the PO results are more accurate than the MM. The loss due to a single reflection at normal incidence for this coating should be 21.18 dB and the loss due to a double reflection at 45° to each reflecting surface should be 28.34 dB. At $\phi = 180°$, which corresponds to the maximum loss due to double reflection, the PO model predicts a loss of 29.02 dB between the RCS for the perfectly conducting geometry in Fig. 4 and the RCS for the coated geometry in Fig. 5. The MM predicts a loss of 29.73 dB at this same point. At $\phi = 135°$, which corresponds to normal incidence to Plate II and, thus, maximum loss due to a single reflection, the PO model predicts a loss of 19.53 dB, while the MM model predicts a loss of only 16.64 dB. In addition to being more accurate than the MM model, the PO model is also much faster. The data in Fig. 5 took only a few seconds for the PO model to compute, whereas the MM model took several hours to complete these RCS calculations.

C. FUTURE WORK

In this report, suggestions for improving the UTD model for predicting the RCS of the coated plate were presented along with a PO model for the coated dihedral corner reflection. Both of these structures are important for studying basic scattering mechanisms that must be understood in order to progress to formulating accurate high-frequency models for complicated structures in which multiple reflections and multiple diffractions dominate, or at least contribute significantly to, the overall scattering pattern. Immediate future work on this project will involve completing the coated plate model and obtaining calculated results to validate using experimental data. In addition, the work on the coated dihedral corner reflector will be completed. Specifically, the UTD analysis will be corrected to resolved inaccuracies. Experimental work is in progress and will yield data to be used for validation. Since the accuracy of the MM solution is in question, this measured data will be ex-

tremely important. Other future work will focus on nonprincipal-plane scattering from both uncoated and coated conducting plates. This scattering configuration is useful for studying interaction among skewed edges and corner scattering.

II. A PHYSICAL OPTICS/ EQUIVALENT CURRENTS MODEL FOR THE RCS OF TRIHEDRAL CORNER REFLECTORS

A. INTRODUCTION

In the last report we examined the radar cross section (RCS) of both the square and triangular trihedral corner reflectors in their interior regions. The reflected fields were calculated using a combination of Geometrical Optics (GO) and Physical Optics (PO). Specifically, the expressions for the initial reflected fields were derived using GO and the appropriate boundary conditions on the surface of a perfectly conducting plate; and the final reflected fields were calculated by applying the PO approximation on the plate of last reflection. The surface integration was evaluated in closed-form; therefore, no numerical integration was really necessary. The integrand was simplified considerably using the far-field approximations before the integration was actually performed. Nevertheless, for far-field computations these approximations had negligible effect on the final results.

The diffracted fields from the exterior edges of both trihedral corner reflectors were computed using the Method of Equivalent Currents (MEC) based on Michaeli's Physical Theory of Diffraction (PTD) equivalent edge currents, sometimes referred to as PTD-EEC [16, 17]. These are based on the fringe currents that exist at the edges. In other words, the PO current is not included in the expressions of the PTD-EEC; therefore, the diffracted fields are expected to improve upon the RCS formulation based upon the reflected fields alone.

Comparison with experimental and Finite-Diference-Time-Domain (FDTD) data was included in the previous report. For most of the RCS patterns that were obtained based on the above modeling, there was very good to excellent agreement with both experimental and FDTD data. However, for some of the RCS

patterns, especially the conical one, the agreement was not very good. Specifically, at and near the null points the difference was as large as 4 or 5 dB. Also, the height of the two sidelobes at 0° and 90° was sometimes off by 1 or 2 dB. Other minor discrepancies were also observed in some of those patterns. This was the main reason that motivated us to introduce a new approach for more accurately calculating the multiply reflected fields from the three trihedral plates [15]. The improved method utilizes strictly PO for all reflections. However, in order to reduce the CPU time, GO is used for the first reflection of all the triply reflected fields, whereas PO is used for the last two reflections. In the case of doubly reflected fields, PO was applied on both the plates of reflection. Expressions for the single reflections are identical to those implemented by the previous approach already explained in the last two reports.

RCS patterns of trihedral corner reflectors were obtained in the past [18]-[20] by using Physical Optics (PO) and diffraction techniques. In all of these cases [18]-[20], the PO approximation was applied only on the plate of last reflection. At initial reflections Geometrical Optics (GO) was used. For example, the CAD-based Shooting and Bouncing Ray (SBR) method [18], as well as many other multi-purpose computer codes [19], apply GO at consecutive initial reflections to find the fields at an aperture plane. Based on these fields, the surface current density on the aperture is evaluated and then integrated to find the scattered fields. This approach provides fairly good results compared with measurements. It is also important to mention here that in all the above references researchers examined the RCS patterns of the square trihedral only. The only reference to the triangular trihedral was the work by Peters [21] performed in the 1960's.

Improved results can be obtained if GO is not used at initial reflections. The reason is that the GO reflected field is always a plane wave which is usually not a good approximation of the actual reflected field, especially in the near-field region of the plate of reflection. However if PO, instead of GO, is applied at initial reflections, the induced surface current densities on subsequent plates due to these

reflected fields will be more accurate; thus, the scattered fields will be more accurate as well. This approach is valid for any number of multiple reflections. In the case of a trihedral corner reflector, there are single reflections, double reflections, and triple reflections. PO can be applied on both plates for double reflection terms, as well as on all three plates for triple reflections. However, for double reflections the formulations result in a quadruble integration, whereas for triple reflections they result in a six-fold integration. To evaluate these integrations, various numerical integration techniques, such as Gaussian quadrature, can be implemented. However, the computational cost, as well as the computational error, increases as the number of nested integrations increases. For this reason, GO is implemented on the first reflection of a triple bounce in the interior of the trihedral; and PO is applied on the plates of the last two reflections. In other words, a quadruble integration is required by both double and triple reflections. The same approach was also used to improve the RCS patterns of dihedral corner reflectors [15].

In addition to considerable improvements in the RCS patterns, the use of strictly PO on all multiple reflections has the advantage of causing no shaded areas on the second and third plates of the trihedral [20]. The PO reflected fields from a trihedral plate will completely illuminate the other two plates; therefore, discontinuities on the surface current densities are eliminated. In our case, for triple reflections it is still necessary to find the shaded and illuminated areas on the second plate, but not on the third plate. Thus, the surface current density on the plate of last reflection is still continuous. In this analysis, first-order diffractions from the exterior edges of both the triangular and square trihedrals are included as in the previous method already discussed in the last two reports.

B. ANALYSIS: THE IMPROVED METHOD

Contrary to the previous method, which uses GO for initial reflections, the improved method uses strictly PO for all reflections. In other words, the improved

method implements PO on all the trihedral plates for both double and triple reflections. In the case of triple reflections, however, it was decided that GO, instead of PO, should be applied on the plate of first reflection. The reasons for using this formulation method were, first, to reduce the CPU time required for the long computations and, second, to keep the numerical error as small as possible. Simply stated, the improved method uses PO for single reflections, PO-PO for double reflections, and GO-PO-PO for triple reflections.

Using strictly PO for all the reflections, the interior of the trihedral is totally illuminated, not only in the case of single reflections, but also in the case of double and triple reflections as well. Note that the source must be located somewhere in the interior of the trihedral, otherwise shading on the plate of first reflection will always occur. In any case, the reflected fields from the plate of first reflection will still illuminate the other two trihedral plates completely. The fact that shading does not occur when strictly PO is used for all reflections (as long as the source lies in the interior region of the trihedral) is a major advantage of the improved method, as compared to the previous method. The reason is that many of the numerical computations that had been used to find the illuminated and shadowed regions on a particular plate are now not necessary. Consequently, the PO surface integral will always be evaluated on the entire surface of that plate; however, because of the use of GO for the triple reflected fields, it is still necessary to find the illuminated area on the second plate.

Another important advantage of the improved method, as compared to the previous method, is that the reflected fields are now more accurately evaluated. Using the previous method, the initial reflected fields were calculated based on the GO approximation, which assumes that the reflected field from a flat plate is still a plane wave with a direction obtained using the Snell's law of reflection. This is a fairly good approximation, especially as the plate becomes larger; however, when multiple reflections occur, as in the case of a trihedral, the second plate lies in the near-field region of the first plate, and consequently the reflected field cannot

be considered exactly a plane wave. On the other hand, by applying PO on the plate of first reflection, without actually using the far-field approximation on the radiation integral, the reflected field in the near-field region of the first plate can be calculated more accurately. Therefore, the surface current density on the second plate, which is twice the reflected magnetic field from the first plate, is now a better approximation of the actual currents on that plate. In addition, the surface current density, obtained using the improved method, does not exhibit any discontinuities as was the case with the previous method. However, the integrations in such a method can only be evaluated numerically. This is a major drawback of the improved method. Another drawback is that multiple reflections require multi-fold integrations which cannot be evaluated very accurately and quickly using current computers and numerical techniques. However, in the case of a trihedral corner reflector, the improved method requires evaluation of double and quadruble integrations only. Evaluation of a six-fold integration would be necessary if strictly PO were used for the triple reflections. Note that the formulation of the strictly PO triple reflected fields is not as difficult as the numerical evaluation of a six-fold integration.

The formulations of a double and a triple reflected field, using the improved method, are given explicitly in the following subsections. Expressions for the rest of the reflected components can be derived following a similar procedure. The formulations for the singly reflected fields are the same as those derived for the previous method. Also, it is important to note that the following expressions are valid only when the plane wave source lies in the interior region of the trihedral. Although not very difficult to formulate, the RCS from the exterior region of the trihedral is not calculated using this improved method.

1. Double Reflection Formulation (Plate 1 to Plate 2)

The incident plane wave magnetic field in the interior of either the square or the triangular trihedral corner reflector is given by

$$\mathbf{H_1^i} = (-\hat{\mathbf{a}}_x \sin\phi_i + \hat{\mathbf{a}}_y \cos\phi_i) H_o e^{jkL_i} \tag{6a}$$

$$L_i = x\sin\theta_i\cos\phi_i + y\sin\theta_i\sin\phi_i + z\cos\theta_i \tag{6b}$$

Equation (6a) is evaluated, according to the PO approximation, on the surface of plate 1 in order to find the surface current density on that plate. This results in

$$\mathbf{J_1} = -2H_o(\hat{\mathbf{a}}_x \cos\phi_i + \hat{\mathbf{a}}_y \sin\phi_i) e^{jk(x''\sin\theta_i\cos\phi_i + y''\sin\theta_i\sin\phi_i)} \tag{7}$$

The magnetic vector potential $\mathbf{A}$ can then be found using the following radiation surface integral:

$$\mathbf{A_1} = \frac{\mu}{4\pi}\int\int \mathbf{J_1}\frac{e^{-jkR''}}{R''}dx''dy'' \tag{8a}$$

$$R'' = \sqrt{(x'-x'')^2 + (y'-y'')^2 + (z'-z'')^2} \tag{8b}$$

where $''$ denotes a point on the surface of integration, and $'$ denotes the observation point. Also, note that $z'' = 0$ since the above integration is evaluated on the surface of plate 1. Substituting equation (7) into equation (8a) results in

$$\begin{aligned}\mathbf{A_1} &= \frac{-H_o\mu}{2\pi}(\hat{\mathbf{a}}_x\cos\phi_i + \hat{\mathbf{a}}_y\sin\phi_i) \\ &\times \int\int e^{jk(x''\sin\theta_i\cos\phi_i + y''\sin\theta_i\sin\phi_i)}\frac{e^{-jkR''}}{R''}dx''dy''\end{aligned} \tag{9}$$

The reflected magnetic field from plate 1 can be found by taking the curl of the magnetic vector potential $\mathbf{A_1}$.

$$\mathbf{H_1} = \frac{1}{\mu}\nabla\times\mathbf{A_1} \tag{10}$$

In rectangular coordinates, equation (10) can be written as

$$\begin{aligned}\mathbf{H_1} &= \frac{1}{\mu}\left[\hat{\mathbf{a}}_x\left(\frac{\partial\mathbf{A}_{1z}}{\partial y'} - \frac{\partial\mathbf{A}_{1y}}{\partial z'}\right)\right. \\ &+ \left.\hat{\mathbf{a}}_y\left(\frac{\partial\mathbf{A}_{1x}}{\partial z'} - \frac{\partial\mathbf{A}_{1z}}{\partial x'}\right) + \hat{\mathbf{a}}_z\left(\frac{\partial\mathbf{A}_{1y}}{\partial x'} - \frac{\partial\mathbf{A}_{1x}}{\partial y'}\right)\right]\end{aligned} \tag{11}$$

However, in the case of the double reflection from plate 1 to plate 2

$$\mathbf{A}_{1z} = 0 \tag{12}$$

Therefore,

$$\mathbf{H_1} = \frac{1}{\mu}\left[-\hat{\mathbf{a}}_x \frac{\partial \mathbf{A}_{1y}}{\partial z'} + \hat{\mathbf{a}}_y \frac{\partial \mathbf{A}_{1x}}{\partial z'} + \hat{\mathbf{a}}_z \left(\frac{\partial \mathbf{A}_{1y}}{\partial x'} - \frac{\partial \mathbf{A}_{1x}}{\partial y'}\right)\right] \tag{13}$$

The partial derivatives in equation (13) are taken with respect to x', y', z' thus $\mathbf{H_1}$ can be written as

$$\begin{aligned} \mathbf{H_1} &= \frac{H_o}{2\pi}\int\int e^{jk(x''\sin\theta_i\cos\phi_i + y''\sin\theta_i\sin\phi_i)}\left[\hat{\mathbf{a}}_x \sin\phi_i \frac{\partial Q}{\partial z'}\right. \\ &- \left.\hat{\mathbf{a}}_y \cos\phi_i \frac{\partial Q}{\partial z'} - \hat{\mathbf{a}}_z\left(\sin\phi_i \frac{\partial Q}{\partial x'} + \cos\phi_i \frac{\partial Q}{\partial y'}\right)\right] dx''dy'' \end{aligned} \tag{14}$$

where Q is defined as

$$Q = \frac{e^{-jkR''}}{R''} \tag{15}$$

Note that the integration is over the entire surface of plate 1 since it is totally illuminated by the source. In other words, the surface of integration is either a square, for a square trihedral, or a triangle, for a triangular trihedral. The partial derivatives in equation (15) with respect to x', y', z' can be found in a straightforward way.

Let us first consider the partial derivative of Q with respect to x'.

$$\frac{\partial Q}{\partial x'} = \frac{\partial Q}{\partial R''} \cdot \frac{\partial R''}{\partial x'} \tag{16a}$$

$$\frac{\partial Q}{\partial R''} = \frac{(-jkR'' - 1)\cdot e^{-jkR''}}{R''^2} \tag{16b}$$

$$\frac{\partial R''}{\partial x'} = \frac{(x' - x'')}{R''} \tag{16c}$$

Based on the above formulation, therefore, we can write the final expressions of the partial derivatives of Q with respect to x', y', and z':

$$\frac{\partial Q}{\partial x'} = \frac{(-jkR'' - 1)\cdot e^{-jkR''}}{R''^2} \cdot \frac{(x' - x'')}{R''} \tag{17a}$$

$$\frac{\partial Q}{\partial y'} = \frac{(-jkR'' - 1) \cdot e^{-jkR''}}{R''^2} \cdot \frac{(y' - y'')}{R''} \tag{17b}$$

$$\frac{\partial Q}{\partial z'} = \frac{(-jkR'' - 1) \cdot e^{-jkR''}}{R''^2} \cdot \frac{(z' - z'')}{R''} \tag{17c}$$

Substituting equations (17a),(17b), and (17c) into equation (14) the reflected magnetic field from plate 1 becomes

$$\begin{aligned} \mathbf{H_1} &= \frac{H_o}{2\pi} \int\int e^{jk(x'' \sin\theta_i \cos\phi_i + y'' \sin\theta_i \sin\phi_i)} \frac{(-jkR'' - 1)}{R''^2} \cdot \frac{e^{-jkR''}}{R''} \\ &\times \{\hat{\mathbf{a}}_x \sin\phi_i (z' - z'') - \hat{\mathbf{a}}_y \cos\phi_i (z' - z'') \\ &- \hat{\mathbf{a}}_z [\sin\phi_i (x' - x'') + \cos\phi_i (y' - y'')]\} \, dx'' dy'' \end{aligned} \tag{18}$$

Knowing the reflected magnetic field from plate 1, we can easily find the surface current density on any of the other two trihedral plates using the PO approximation. However, since we are interested in the double reflected fields from plate 1 to plate 2, only the surface current density on plate 2 is required here.

$$\mathbf{J}_{12} = 2\hat{\mathbf{a}}_x \times \mathbf{H}_1 \tag{19a}$$

$$\begin{aligned} \mathbf{J}_{12} &= \frac{H_o}{\pi} \int\int e^{jk(x'' \sin\theta_i \cos\phi_i + y'' \sin\theta_i \sin\phi_i)} \frac{(-jkR'' - 1)}{R''^2} \cdot \frac{e^{-jkR''}}{R''} \\ &\times \{-\hat{\mathbf{a}}_y [\sin\phi_i (x' - x'') + \cos\phi_i (y' - y'')] + \hat{\mathbf{a}}_z \cos\phi_i (z' - z'')\} \\ &\times dx'' dy'' \end{aligned} \tag{19b}$$

$$z'' = 0 \tag{19c}$$

$$x' = 0 \tag{19d}$$

Using the surface current density on plate 2 due to the double reflected field component R_{12} we can find the magnetic vector potential $\mathbf{A}_{12}$.

$$\mathbf{A}_{12} = \frac{\mu}{4\pi} \int\int \mathbf{J}_{12} \frac{e^{-jkR'}}{R'} dy' dz' \tag{20a}$$

$$R' = \sqrt{(x - x')^2 + (y - y')^2 + (z - z')^2} \tag{20b}$$

This double integration is evaluated on the surface of plate 2. The $\prime$ denotes any point on the surface of integration, whereas the x, y, and z denote the position of the observation point which is actually the receiver. Substituting (19b) into (20a) results in the following quadruple integration:

$$\begin{aligned}
\mathbf{A}_{12} &= \frac{H_o \mu}{4\pi^2} \int\int\int\int e^{jk(x'' \sin\theta_i \cos\phi_i + y'' \sin\theta_i \sin\phi_i)} \frac{(-jkR'' - 1)}{R''^2} \cdot \frac{e^{-jkR''}}{R''} \\
&\times \{-\hat{\mathbf{a}}_y [\sin\phi_i (x' - x'') + \cos\phi_i (y' - y'')] + \hat{\mathbf{a}}_z \cos\phi_i (z' - z'')\} \\
&\times \frac{e^{-jkR'}}{R'} dx'' dy'' dy' dz' \qquad (21a)
\end{aligned}$$

$$z'' = 0 \qquad (21b)$$

$$x' = 0 \qquad (21c)$$

The first double integration is evaluated on the surface of plate 1, whereas the second double integration is evaluated on the surface of plate 2. Both plates are totally illuminated.

Knowing the magnetic vector potential $\mathbf{A}_{12}$, the double reflected fields can be found using the expressions below, which are valid only for the far-fields:

$$E_\theta = -j\omega A_\theta \qquad (22a)$$

$$E_\phi = -j\omega A_\phi \qquad (22b)$$

where

$$A_\theta = \cos\theta \cos\phi A_x + \cos\theta \sin\phi A_y - \sin\theta A_z \qquad (22c)$$

$$A_\phi = -\sin\phi A_x + \cos\phi A_y \qquad (22d)$$

2. Triple Reflection Formulation - Plate 1 to Plate 2 to Plate 3

Expressions for the triply reflected fields of a trihedral corner reflector can be derived in a very similar manner to those already derived for the doubly reflected fields. Instead of having a quadruple integration, the final expression will consist

of a six-fold integration since PO is applied on all three trihedral plates. However, in the improved method it was decided to apply GO on the plate of first reflection in order to reduce the six-fold integration to a quadruple integration. The reason is that a six-fold integration is very difficult to accurately evaluate using even the most advanced computers.

Applying GO on the plate of first reflection causes shadow regions on the second plate. This results in discontinuities in the surface current density that is induced on the second plate due to the reflected fields from the first plate. Therefore, even in the improved method we are required to compute the illuminated-shadow boundaries on the second plate due to triply reflected fields. However, we are not required to compute the shading on the third plate since PO, instead of GO, is applied on the second plate. The reflected field from the second plate completely illuminates the third plate; thus, the surface current density is continuous and nonzero at all points on the surface of the last plate.

Using this approach, the formulation of the triply reflected fields is very similar to the formulation of the doubly reflected fields given previously. The only difference is that the first double integration is evaluated only on the illuminated area of the second plate instead of on its entire surface. The second double integration is evaluated on the entire plate of last reflection, as it was for the doubly reflected fields. The expressions for the triply reflected fields R_{123} are given below.

The incident magnetic field in the interior of the trihedral is given by equation (6a). Applying GO and the appropriate boundary conditions on plate 1, the resulting reflected magnetic field is given by

$$\mathbf{H}_1^r = (-\hat{\mathbf{a}}_x \sin\phi_i + \hat{\mathbf{a}}_y \cos\phi_i) H_o e^{jkL_r} \tag{23}$$

$$L_r = x\sin\theta_i\cos\phi_i + y\sin\theta_i\sin\phi_i - z\cos\theta_i \tag{24}$$

The surface current density on the illuminated area of the second plate is then formed using the PO approximation:

$$\mathbf{J}_{12} = \hat{\mathbf{a}}_z 2H_o \cos\phi_i e^{jk(y''\sin\theta_i\sin\phi_i - z''\cos\theta_i)} \tag{25}$$

On the shadowed area of the second plate, the surface current density, according to PO, is zero. The corresponding magnetic vector potential and the reflected magnetic field from plate 2 are:

$$\mathbf{A}_{12} = \hat{\mathbf{a}}_z \cos\phi_i \frac{H_o \mu}{2\pi} \int\int e^{jk(y'' \sin\theta_i \sin\phi_i - z'' \cos\theta_i)} \cdot \frac{e^{-jkR''}}{R''} dx'' dy'' \tag{26}$$

$$\begin{aligned} \mathbf{H}_{12} &= \frac{H_o}{2\pi} \int\int e^{jk(y'' \sin\theta_i \sin\phi_i - z'' \cos\theta_i)} \frac{(-jkR'' - 1)}{R''^2} \cdot \frac{e^{-jkR''}}{R''} \\ &\times \{\hat{\mathbf{a}}_x \cos\phi_i (y' - y'') - \hat{\mathbf{a}}_y \cos\phi_i (x' - x'')\} \, dy'' dz'' \end{aligned} \tag{27}$$

The integrations in both the above two expressions are evaluated only over the illuminated area of plate 2. Note also that x'' is zero in equations (26) and (27).

Using the expression for $\mathbf{H}_{12}$, the surface current density on plate 3 can be found by using the PO approximation:

$$\begin{aligned} \mathbf{J}_{123} &= -\hat{\mathbf{a}}_z \frac{H_o}{\pi} \cos\phi_i \int\int e^{jk(y'' \sin\theta_i \sin\phi_i - z'' \cos\theta_i)} \frac{(-jkR'' - 1)}{R''^2} \cdot \frac{e^{-jkR''}}{R''} \\ &\times (y' - y'') dy'' dz'' \end{aligned} \tag{28}$$

In equation (28) both x'' and y' are zero. Knowing the surface current density on the third plate due to the triple reflected fields R_{123}, we can easily formulate the magnetic vector potential $\mathbf{A}$:

$$\begin{aligned} \mathbf{A}_{123} &= -\hat{\mathbf{a}}_z \frac{H_o \mu}{4\pi^2} \cos\phi_i \int\int\int\int e^{jk(y'' \sin\theta_i \sin\phi_i - z'' \cos\theta_i)} \frac{(-jkR'' - 1)}{R''^2} \cdot \frac{e^{-jkR''}}{R''} \\ &\times (y' - y'') \frac{e^{-jkR'}}{R'} dy'' dz'' dx' dz' \end{aligned} \tag{29a}$$

$$R' = \sqrt{(x - x')^2 + (y - y')^2 + (z - z')^2} \tag{29b}$$

$$x'' = 0 \tag{29c}$$

$$y' = 0 \tag{29d}$$

The quadruple integration must be evaluated numerically since there is no closed form solution to it. Gaussian quadrature was implemented in our computer programs to carry out this integral. Sixteen or more evaluation points usually gives

an acceptable answer. Increasing the number of points in the Gaussian quadrature subroutine always improves the accuracy of the results; however, the computational cost also increases. The above equations are incorporated into the far-field expressions to find the triply reflected fields from the interior of either the square or the triangular trihedral. Note that the surface of integration will be different in various cases.

C. RESULTS

RCS results based on the above formulations were obtained for both the square and triangular trihedral corner reflectors, shown in Fig. 6, for the E_θ polarization. Fig. 7 shows the RCS of a 5λ square trihedral for an incident angle $\theta = 66^o$. Fig. 8 shows the RCS of a 10λ triangular trihedral for an incident angle $\theta = 70^o$. Both graphs show considerable improvements compared to those obtained using GO at all initial reflections and PO only at the plate of last reflection; however, the improved method requires more computational time than the previous method.

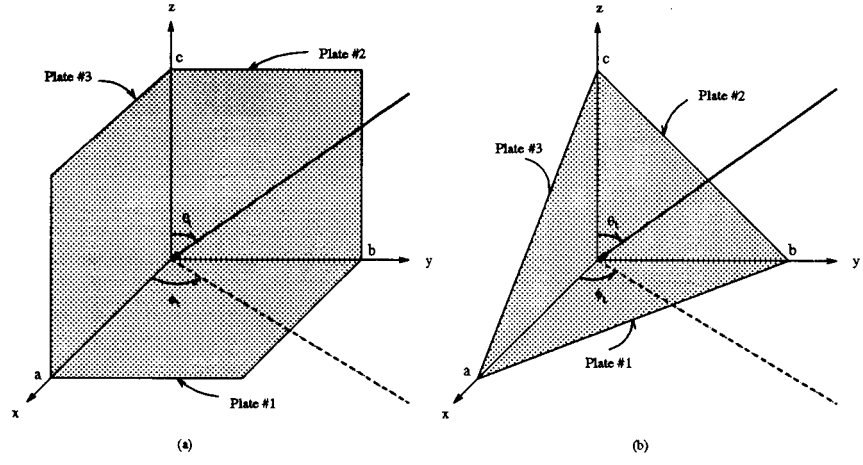

Figure 6: Geometry of the square and triangular trihedral corner reflectors.

D. CONCLUSIONS

In this report we have introduced a new approach to the RCS calculation of trihedral corner reflectors. Both the square and triangular trihedrals were examined.

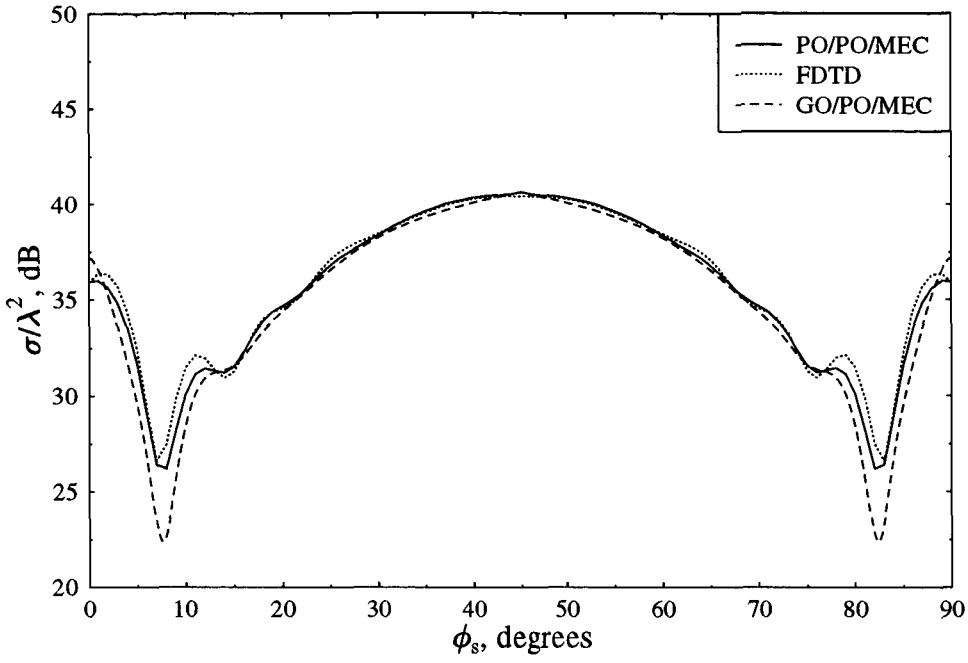

Figure 7: Monostatic RCS of the square trihedral with dimensions $a = b = c = 5.0\lambda$, incident angle $\theta = 66°$, and E_θ polarization.

Comparisons show that the results obtained with the new approach yield better agreement with experimental and/or FDTD data than the results obtained with the old approach, which was discussed extensively in the last two reports. The new approach, however, has a major drawback in that it requires more CPU time than the old approach. This is due to the fact that all the surface integrations are evaluated numerically. In addition, for double and triple reflections we need to evaluate a quadruple integration which requires four nested single integration routines. As a result, the CPU time, as well as the numerical error, increases considerably. The CPU time required to evaluate a numerical integration increases with the number of points considered in the Gaussian quadrature. The accuracy of the results also improves as the number of the evaluation points increases. Good results were obtained with a 16-point Gaussian quadrature.

The only possible way to reduce the CPU time required, as well as the numerical error, is to break the integrand into two separate functions so that the

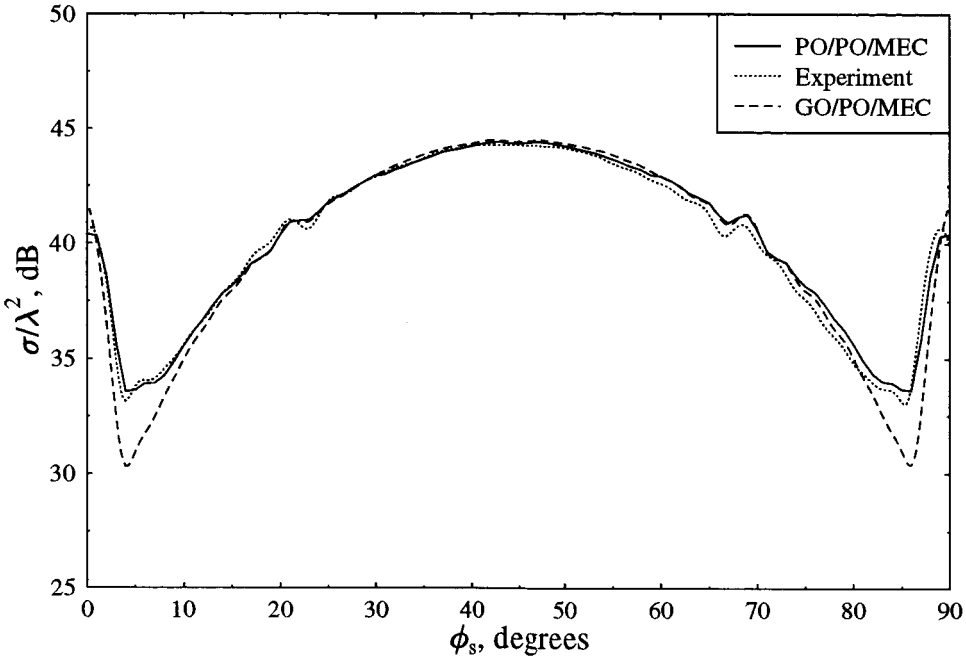

Figure 8: Monostatic RCS of the triangular trihedral with dimensions $a = b = c = 10.0\lambda$, incident angle $\theta = 70°$, and E_θ polarization.

evaluation of the quadruble integration becomes simply a multiplication of two double integrations. This, however, is a very challenging task to carry out because of the complexity of the integrand.

References

[1] C. A. Balanis, L. A. Polka, and A. C. Polycarpou, "High-frequency techniques for RCS prediction of plate geometries and a physical optics/equivalent currents model for the RCS of trihedral corner reflectors," Semiannual Report, Grant No. NAG-1-562, National Aeronautics and Space Administration, Langley Research Center, Hampton, VA, Jul. 31, 1993.

[2] C. A. Balanis, L. A. Polka, and A. C. Polycarpou, "High-frequency techniques for RCS prediction of plate geometries and a physical optics/equivalent currents model for the RCS of trihedral corner reflectors," Semiannual Report, Grant No. NAG-1-562, National Aeronautics and Space Administration, Langley Research Center, Hampton, VA, Jan. 31, 1993.

[3] C. A. Balanis and L. A. Polka, "High-frequency techniques for RCS prediction of plate geometries," Semiannual Report, Grant No. NAG-1-562, National

Aeronautics and Space Administration, Langley Research Center, Hampton, VA, Jul. 31, 1992.

[4] C. A. Balanis and L. A. Polka, "High-frequency techniques for RCS prediction of plate geometries," Semiannual Report, Grant No. NAG-1-562, National Aeronautics and Space Administration, Langley Research Center, Hampton, VA, Jan. 31, 1992.

[5] C. A. Balanis and L. A. Polka, "High-frequency techniques for RCS prediction of plate geometries," Semiannual Report, Grant No. NAG-1-562, National Aeronautics and Space Administration, Langley Research Center, Hampton, VA, Jul. 31, 1991.

[6] C. A. Balanis and L. A. Polka, "High-frequency techniques for RCS prediction of plate geometries," Semiannual Report, Grant No. NAG-1-562, National Aeronautics and Space Administration, Langley Research Center, Hampton, VA, Jan. 31, 1991.

[7] C. A. Balanis, L. A. Polka, and K. Liu, "Scattering from coated structures and antenna pattern control using impedance surfaces," Semiannual Report, Grant No. NAG-1-562, National Aeronautics and Space Administration, Langley Research Center, Hampton, VA, Jul. 31, 1990.

[8] C. A. Balanis, L. A. Polka, and K. Liu, "Nonprincipal plane scattering from rectangular plates and pattern control of horn antennas," Semiannual Report, Grant No. NAG-1-562, National Aeronautics and Space Administration, Langley Research Center, Hampton, VA, Jan. 31, 1990.

[9] R. Tiberio, G. Pelosi, and G. Manara, "A uniform GTD formulation for the diffraction by a wedge with impedance faces," *IEEE Trans. Antennas Propagat.*, vol. AP-33, pp. 867 – 873, Aug. 1985.

[10] T. Griesser and C. A. Balanis, "Reflections, diffractions, and surface waves for an interior impedance wedge of arbitrary angle," *IEEE Trans. Antennas Propagat.*, vol. AP-37, pp. 927 – 935, Jul. 1989.

[11] T. Griesser, C. A. Balanis, and K. Liu, "RCS analysis and reduction for lossy dihedral corner reflectors," *IEEE Proceedings*, vol. Vol. 77, pp. 806–814, May 1989.

[12] T. Griesser, *High-Frequency Electromagnetic Scattering from Imperfectly Conducting Structures.* PhD thesis, Arizona State University, Tempe, Arizona, Aug. 1988.

[13] R. Tiberio, G. Pelosi, G. Manara, and P. Pathak, "High-frequency scattering from a wedge with impedance faces illuminated by a line source, Part I:

Diffraction," *IEEE Trans. Antennas Propagat.*, vol. AP-37, pp. 212–218, Feb. 1989.

[14] G. Manara, R. Tiberio, G. Pelosi, and P. Pathak, "High-frequency scattering from a wedge with impedance faces illuminated by a line source, Part II: Surface waves," *IEEE Trans. Antennas Propagat.*, vol. AP-41, pp. 877–883, Jul. 1993.

[15] T. Griesser and C. A. Balanis, "Backscatter analysis of dihedral corner reflectors using physical optics and the physical theory of diffraction," *IEEE Trans. Antennas Propagat.*, vol. AP-35, pp. 1137–1147, Oct. 1987.

[16] A. Michaeli, "Equivalent edge currents for arbitrary aspects of observation," *IEEE Trans. Antennas Propagat.*, vol. AP-32, pp. 252–258, Mar. 1984.

[17] A. Michaeli, "Elimination of infinities in equivalent edge currents, Part I: Fringe currents," *IEEE Trans. Antennas Propagat.*, vol. AP-34, pp. 912–918, Jul. 1986.

[18] J. Baldauf, S. W. Lee, L. Lin, S. K. Jeng, S. M. Scarborough, and C. L. Yu, "High frequency scattering from trihedral corner reflectors and other benchmark targets: SBR versus experiment," *IEEE Trans. Antennas Propagat.*, vol. AP-39, pp. 1345–1351, Sep. 1991.

[19] S. W. Lee and R. J. Marhefka, *Data Book of High-Frequency RCS.* Compiled by High Frequency Subgroup of EM Code Consortium, Aug. 1989.

[20] A. C. Polycarpou, C. A. Balanis, and P. A. Tirkas, "Radar cross section evaluation of the square trihedral corner reflector using PO and MEC," *IEEE Antennas Propagat. Soc. Intl. Symp.*, vol. 3, pp. 1428–1431, Jun. 1993.

[21] L. Peters, "Passive bistatic radar enhancement devices," *IEE Proc.*, vol. 109, pp. 1–10, Jul. 1961.